Enhancing the Sensitivity of Biotinylated Surfaces by Tailoring the Design of the Mixed Self-Assembled Monolayer Synthesis

Davide Blasi,◆ Lucia Sarcina,◆ Angelo Tricase,◆ Angela Stefanachi, Francesco Leonetti,* Domenico Alberga, Giuseppe Felice Mangiatordi,* Kyriaki Manoli, Gaetano Scamarcio, Rosaria Anna Picca,* and Luisa Torsi
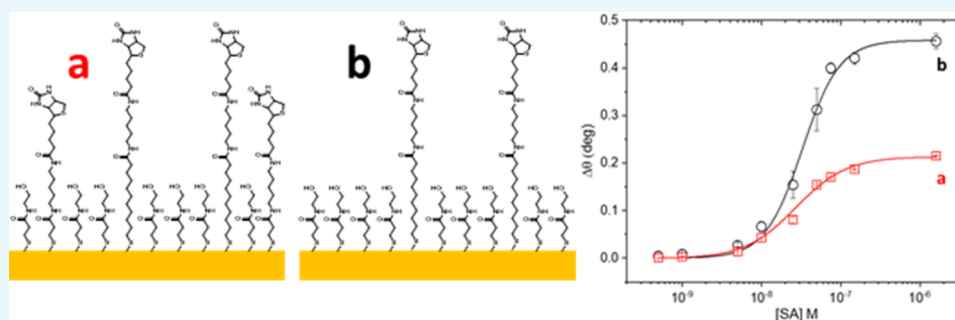
ACCESS | 📊 Metrics & More | 📰 Article Recommendations | 🅢 Supporting Information

ABSTRACT: Thiolated self-assembled monolayers (SAMs) are typically used to anchor on a gold surface biomolecules serving as recognition elements for biosensor applications. Here, the design and synthesis of N-(2-hydroxyethyl)-3-mercaptopropanamide (NMPA) in biotinylated mixed SAMs is proposed as an alternative strategy with respect to on-site multistep functionalization of SAMs prepared from solutions of commercially available thiols. In this study, the mixed SAM deposited from a 10:1 solution of 3-mercaptopropionic acid (3MPA) and 11-mercaptoundecanoic acid (11MUA) is compared to that resulting from a 10:1 solution of NMPA:11MUA. To this end, surface plasmon resonance (SPR) and attenuated total reflectance infrared (ATR-IR) experiments have been carried out on both mixed SAMs after biotinylation. The study demonstrated how the fine tuning of the SAM features impacts directly on both the biofunctionalization steps, i.e., the biotin anchoring, and the biorecognition properties evaluated upon exposure to streptavidin analyte. Higher affinity for the target analyte with reduced nonspecific binding and lower detection limit has been demonstrated when NMPA is chosen as the more abundant starting thiol. Molecular dynamics simulations complemented the experimental findings providing a molecular rationale behind the performance of the biotinylated mixed SAMs. The present study confirms the importance of the functionalization design for the development of a highly performing biosensor.

INTRODUCTION

The functionalization strategy of a detecting interface is critical to build a robust and highly performing biosensing platform.[1] Indeed, the active surface involved in the recognition of a given biomarker is a key element that needs to be carefully designed. Above all, the specific binding should be guaranteed with minimal influence from background interferences once the sensor assays complex matrices such as real fluids. In general, both physical and chemical methods can be used to immobilize a biomolecule on a surface. Among others, self-assembly has been widely proven to be particularly effective.[2] Indeed, self-assembled monolayers (SAMs)[3] are known as one of the main routes to tune surface properties (e.g., chemical reactivity, conductivity, and biocompatibility) of a given interface.[4] In particular, thiol-based SAMs[5] represent a convenient strategy to anchor biorecognition elements on gold surfaces and nanostructures[1,6] for sensing applications.[7] Relevantly, they are becoming a key feature to be considered in developing ultrasensitive biosensors based on functionalized interphases.[8−11] Actually, if, on the one hand, the main task of a SAM is to assure a reproducible immobilization of a biomolecule on a surface, then, on the other hand, tailoring the SAM architecture is critically important to control the biorecognition capability and, hence, the analytical performance of a biosensor.[12,13] Especially, the co-adsorption of a mixture of two alkyl thiols results in the growth of mixed SAMs on gold surfaces, which is recognized as particularly effective and so widely reported as a successful strategy.[14−18] In this
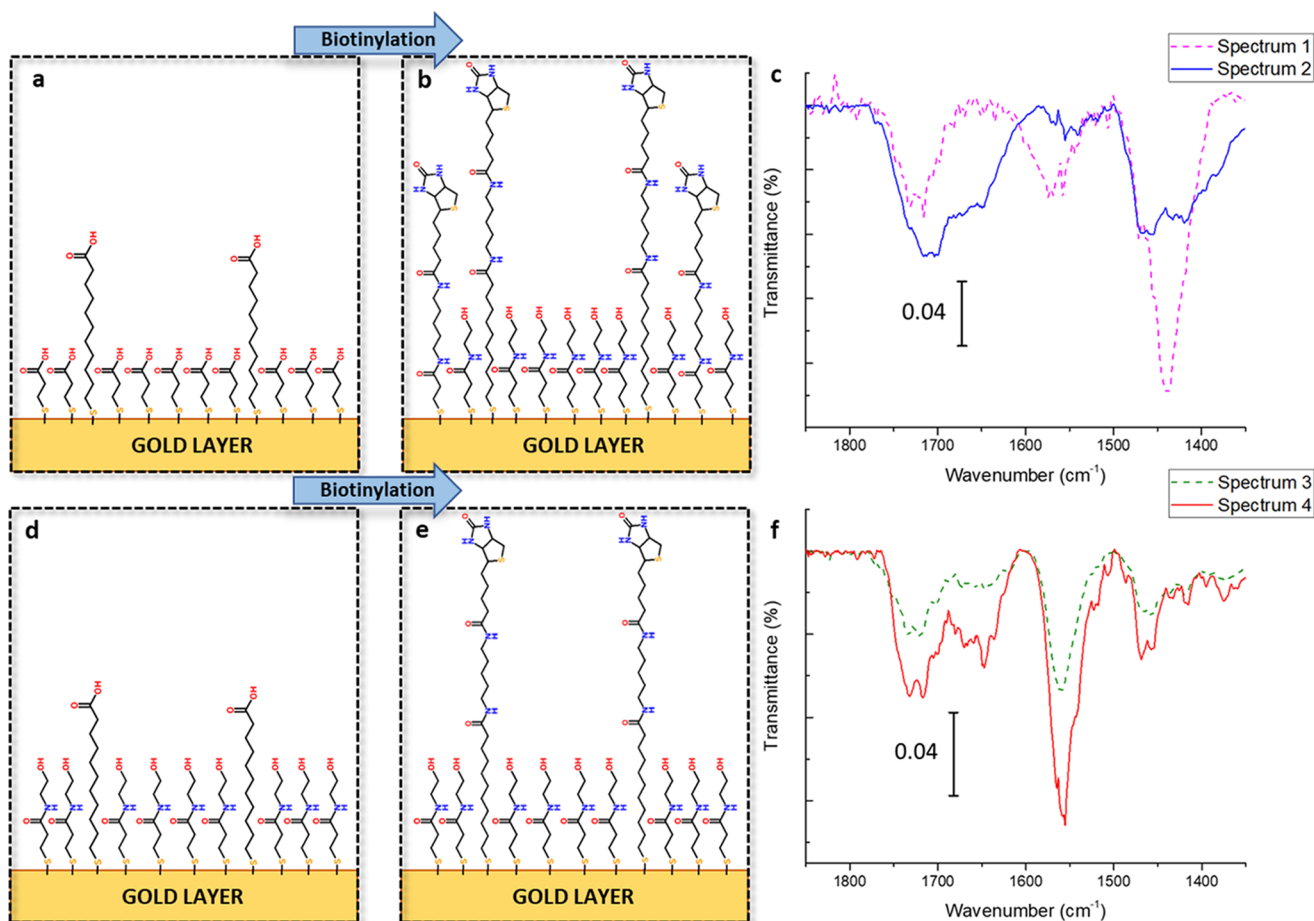
Figure 1. Schematic representation of the mixed SAMs (a, d) before and (b, e) after the biotin conjugation together with (c, f) the corresponding ATR-IR spectra in the range of 1850−1350 cm^{-1}. Panels (a) and (b) refer to the 3MPA:11MUA SAM before and after biotinylation, respectively; the corresponding ATR-IR spectra (1) and (2) are given in panel (c). Panels (d) and (e) show the scheme of NMPA:11MUA SAM before and after biotinylation, respectively; the corresponding ATR-IR spectra (3) and (4) are given in panel (f).

case, a solution of two distinct alkyl thiols, which may differ for the aliphatic chain length and/or the functional terminal group, is used. Typically, the longer chain serves to anchor the biorecognition element and is used in a more diluted concentration, whereas the shorter one acts as a dilution thiolate.[19,20] In fact, the latter serves as a spacer tuning the distance among contiguous biorecognition elements. Such an occurrence prevents two neighboring biomolecules from hindering each other in binding the analyte, thus enhancing the binding efficacy.[19,20] Eventually, a suitable orientation of the biorecognition element on the surface can be achieved as well. Moreover, immobilization should be quantitative without significant alteration of the biomolecule binding properties. As a result, the proper choice of thiol structure and length and the molar ratio between anchoring and dilution thiols have been systematically studied to develop *ad hoc* designed biosensors, demonstrating how they can affect the orientation of the bioreceptor and hence its capability to detect the target analyte.[21−23] Indeed, the degree of the order of the biofunctionalized SAM is also a critical aspect that should be taken into account for improving the sensitivity of a biosensor.

In our recent work on electrolyte-gated organic field effect transistor (EGOFET) biosensors,[8,11,24−26] a mixed SAM deposited from a solution of 11-mercaptoundecanoic acid (11MUA) and 3-mercaptopropionic acid (3MPA) in molar ratio of 1:10 was used. The proposed ratio has been generally

reported as the most favorable proportion to get a higher surface coverage of bioreceptors (e.g., proteins, enzymes, and antibodies) as compared to single-component SAMs.[15,27,28] Moreover, a homogeneous mixed SAM can be prepared from ethanolic solutions.[29] According to the literature,[15] this would lead to a highly packed layer of antibodies. The biofunctionalization process was carried out by activating the carboxylic moieties of 3MPA:11MUA SAMs through 1-ethyl-3-(3-dimethylaminopropyl)carbodiimide/N-hydroxysulfosuccinimide sodium salt (EDC/NHSS) coupling.[15] This enables the antibodies to conjugate to the SAM. Finally, the unreacted carboxylic groups are blocked by exposure to an excess of ethanolamine[24] (Figure S1). This procedure gave no control on where the antibody would attach and, indeed, it could anchor either to the activated 11MUA or the activated 3MPA. It could be speculated that the longer and more flexible 11MUA chain would make it easier for the antibody to attach.

In the last step of the biofunctionalization process, the *N*-(2-hydroxyethyl)-3-mercaptopropanamide (NMPA) compound is formed *in situ*, replacing the originally present 3MPA. The NMPA structure can enable the formation of an extended hydrogen-bonding network,[30−32] involving the oxygen of the amide group in one NMPA chain and the hydrogen of the amide group of a neighboring one, which could be important for the unprecedented sensitivity of the developed EGOFET biosensors.[8] As described, the NMPA is synthesized directly *in*

situ at the gold surface following a multiple-step protocol. It is, however, a fact that an *in situ* synthesis does not provide any control over the yield of the amide production or the degree of order of the SAM. This could impact on the device performance. The implementation of a more controlled SAM architecture that results in a better-ordered layer might lead even to higher sensitivity. To this end, a strategy involving a mixed SAM that starts from *ex situ* synthesized NMPA was adopted. The *ad hoc* synthesized NMPA in place of 3MPA as dilution thiol (acting only as such in this configuration) served to deposit the NMPA:11MUA 10:1 mixed SAMs featured in Figure S2. The aim of this work is to compare the functionalization strategies resulting in the 3MPA:11MUA and NMPA:11MUA mixed SAMs in terms of sensing performance. The literature on amide-based hydrogen bonds within SAMs is rather limited[32−35] despite the fact that it has been proven that SAMs bearing amide moieties lead to more robust and stable surfaces suitable for further modification and biofunctionalization.[34] This work provides further compelling evidence of the validity of such an approach with the support of several characterization tools. As a proof of concept, biotin was selected as the biorecognition element and streptavidin (SA) as the target analyte as the biotin−streptavidin couple generates one of the strongest biological interactions and can serve as an effective model system in the study of a novel biosensing platform.[36,37] The syntheses of different biotinylated thiols serving as binding units in SAMs have been proposed to study the impact of a better-ordered SAM structure on streptavidin binding.[13,38,39] To control the spacing between the biotinylated and dilution thiols, a proposed strategy involves biotinylation to be carried out before depositing the SAMs. For example, Nelson et al.[39] proposed the use of methyl- or oligo(ethylene oxide)-terminated thiols as diluents. Though both molecules could promote a certain degree of order in the mixed SAMs, it was found that the SAM surface composition differed from the solution mixing ratio. Additionally, the alkyl-terminated diluent caused an increase in the nonspecific binding of streptavidin. In the present work, a different strategy is adopted to tackle the formation of a better-ordered SAM structure; in this respect, NMPA plays a critical role in reducing nonspecific binding of streptavidin and increasing the sensitivity toward this biomolecule. To this aim, biotinylated gold surfaces were prepared using the two different mixed SAMs (starting SAMs reported in Figure 1a,d) in order to assess if better control over the conjugation of the biorecognition elements could enable better sensing performance. As already highlighted, when the 3MPA:11MUA mixed SAM was used, biotin could conjugate to both activated mercaptocarboxylic acids, thus leading to surfaces with a higher number of biorecognition molecules but with a less controlled structure. By contrast, the use of NMPA allows the biotinylation only to occur on the 11MUA chain. A schematic representation of the biotinylated surfaces based on the 3MPA:11MUA and NMPA:11MUA SAMs is shown in Figure 1b,e.

Spectroscopic and optical methods were used to study these surfaces. Specifically, a combination of attenuated total reflection infrared (ATR-IR) spectroscopy and surface plasmon resonance (SPR) experiments was employed to investigate the differences in the layer composition and their response to SA exposure providing information on the influence of the functionalization protocol on the sensing performance level. Finally, molecular dynamics (MD)

simulations were carried out to provide a molecular rationale behind the observed different performance. Taken as a whole, the obtained data represent an unprecedented starting point for driving the rational design of biotinylated mixed SAMs.

■ EXPERIMENTAL SECTION

Streptavidin from *Streptomyces avidinii* and bovine serum albumin (BSA) were purchased from Sigma-Aldrich, whereas pentylamine-biotin was from Thermo Scientific. 3-mercapto-propionic acid (3MPA) (98%), 11-mercaptoundecanoic acid (11MUA), *N*-hydroxysulfosuccinimide sodium salt (NHSS), 1-ethyl-3-(3-dimethylamino-propyl)carbodiimide (EDC), and ethanolamine hydrochloride (EA) were purchased from Sigma-Aldrich and used without further purification. 2-(*N*-morpholino)ethane-sulfonic acid (MES) buffer (Sigma-Aldrich) of 0.1 M was adjusted with sodium hydroxide solution (NaOH 1 M) at pH 4.8−4.9. A phosphate buffered saline (PBS, Sigma-Aldrich) (phosphate buffer of 0.01 M, KCl of 0.0027 M, NaCl of 0.137 M) tablet was dissolved in 200 mL of HPLC water and used upon filtration on a Corning 0.22 μm polyethersulfone membrane. NMPA was synthesized starting from commercial 3MPA, and details on its synthesis are provided in the SI. The starting SAMs (Figure S2) were prepared under similar conditions on commercial gold-coated (50 nm) glass slides (SPR Navi-200). Before modification, the substrates were accurately cleaned in piranha solution (3:1 sulfuric acid/H_2O_2 30%$_w$, caution: strong oxidizing agent) for 5 min, then washed in hot water for 10 min, dried with nitrogen, and treated for 10 min in an ozone cleaner. Slides were then immersed in a 10 mM ethanol solution of 3MPA:11MUA or NMPA:11MUA (10:1 molar ratio) under a nitrogen atmosphere for 20 h at 22 °C.[24] The modified slides were rinsed several times with ethanol and stored in the same solvent until use on the SPR apparatus for the following functionalization steps. The preparation of biotinylated SAMs according to the two protocols is sketched in Figure S6.

A BioNavis multiparameter surface plasmon resonance MP-SPR Navi instrument in the Kretschmann configuration was used for the real time monitoring of biotinylation and biomolecule interactions with the biofunctionalized gold surface (i.e., exposure to increasing concentrations of SA).[40,41] Details about SPR measurements, including biotin immobilization and response to SA, are discussed in the Supporting Information.

ATR-IR analysis was performed using a PerkinElmer Spectrum-Two instrument on the same functionalized gold-coated glass slides used for SPR. The measuring protocol for ATR-IR characterization is described in the Supporting Information.

The starting system for MD simulations was built following the protocol previously described.[8] In particular, the Au(111) surface comprising NMPA chains ($\sqrt{3} \times \sqrt{3}$R30° config-uration) was optimized via periodic density functional theory (DFT).[8] The obtained cell was replicated giving a final system having a size of 132 Å × 122 Å in the *xy* plane (Figure S9a). Starting from this system, five different SAMs were built (Figure S9b). More specifically, SAM-1 reproduces a mixed SAM resulting from a NMPA:11MUA functionalization strategy, while SAM-2, SAM-3, SAM-4, and SAM-5 reproduce mixed SAMs compatible with a 3MPA:11MUA functionaliza-tion strategy and having an increasing number of biotinylated 3MPAs (hereinafter referred to as B-3MPAs) as reported in Table 1. MD simulations were performed using the NAMD

Table 1. Number of B-11MUAs, NMPAs, and B-3MPAs in the Five Simulated Systems

system	B-11MUAs	NMPAs	B-3MPAs
SAM-1	66	654	0
SAM-2	66	491	163
SAM-3	66	436	218
SAM-4	66	327	327
SAM-5	66	0	654

2.13 package.[42] For each system, a 100 ns-long MD simulation at T = 25 °C was performed. All the methodological details of the applied MD protocol are reported in the Supporting Information.

■ RESULTS AND DISCUSSION

In this work, two approaches based on the *ex situ* and *in situ* synthesis of NMPA to develop biotinylated gold surfaces were compared. To this aim, the two biotinylation strategies reported in Figure S6 were investigated by real-time SPR experiments. The SPR sensograms measured on the SAM-modified gold surfaces, shown in Figure S7, evidence the changes in the optical density at all the steps of the biotinylation protocol. The two sensograms show almost identical features for both the 3MPA:11MUA and NMPA:11-MUA SAMs. Indeed, the immobilization of a small molecule like biotin does not lead to appreciable variations in the optical density; hence, it cannot be tackled with enough sensitivity in SPR experiments.[37] Better suited to study the different reactivities of the two surfaces is the ATR-IR spectroscopy. The two SAMs' structures and relevant spectra are compared in Figure 1. In particular, a schematic representation of the 3MPA:11MUA and NMPA:11MUA SAM chemical structures before (Figure 1a,d) and after biotinylation (Figure 1b,e) is shown along with their ATR-IR spectra (Figure 1c,f). The wavenumber positions for all the peaks identified in the spectra are summarized in Table S1.

The ATR-IR spectrum of the 3MPA:11MUA SAM (Figure 1c, spectrum 1) exhibits characteristic features associated with the presence of carboxylic acid moieties: C═O stretching at 1720 cm^{-1}, asymmetric and symmetric carboxylate stretching vibrations at 1570 and 1438 cm^{-1}, respectively. A shoulder around 1470 cm^{-1}, attributed to a methylene bending signal, can be observed close to the carboxylate symmetric stretching band. After biotinylation, the SAM (Figure 1c, spectrum 2) exhibits an intense band between 1750 and 1600 cm^{-1} ascribed to the overlap of several signals. In fact, by comparison with literature data on similar samples[43−45] and spectrum 1, specific contributions can be discriminated. Similarly to the attribution performed in spectrum 1, the C═O stretching, associated with the presence of unreacted carboxylic functionalities, falls at 1720 cm^{-1}. The very broad absorption between 1700 and 1600 cm^{-1} is the result of at least three different components falling in this region (Table S1): the biotin ring C═O stretching[45] at 1699 cm^{-1} and both the aliphatic amide C═O (amide I) stretching[43,44] and N−H bending of the biotin ring[45] at 1651 cm^{-1}. The band centered at 1550 cm^{-1} is assigned to aliphatic amide N−H bending (amide II). Significant differences between spectra 1 and 2 appear also in the 1500−1400 cm^{-1} range as a consequence of the reaction of both 11MUA and 3MPA carboxylic moieties leading to amide formation. In fact, in spectrum 2, the carboxylate symmetric stretching (1438 cm^{-1}) disappears whereas the C−H bending (1460 cm^{-1})

becomes the main peak of this region. A minor peak can be individuated at 1416 ± 1 cm^{-1} being assigned to C−N bending, which is coherent with amide group formation. These signals are compatible with a model featuring a SAM comprising some of the activated carboxylic anchoring groups (succinimidic esters formed during the EDC/NHSS step) that conjugate biotins while others that are deactivated during the reaction with ethanolamine.

The typical ATR-IR spectrum acquired on the NMPA:11-MUA as-deposited SAM (Figure 1f, spectrum 3) exhibits, as expected, features that are characteristic of the aliphatic amidic moieties (amide I band centered at 1650 cm^{-1} and amide II signal at 1560 ± 1 cm^{-1}; Table S1)[30] already present in the as-synthesized NMPA. Quite interestingly, minimal differences are observed at the end of all the biotinylating steps (Figure 1f, spectrum 4) that are ascribed to the low concentration of 11MUA chains. In this case, the 11MUAs are the only available sites for biotin anchoring. Thus, the resulting amount of biotin in this SAM is lower compared with the previous case. Such findings are corroborated by the similarity between spectra 3 and 4 in Figure 1f. In the latter, a clear contribution from biotin ring vibrations is barely distinguishable if compared to spectrum 2 in Figure 1c.

In fact, differences in the two biotinylation protocols can be highlighted when comparing the IR spectral region characteristic of C═O stretching acquired on both biotinylated 3MPA:11MUA (Figure 2a) and NMPA:11MUA (Figure 2b)
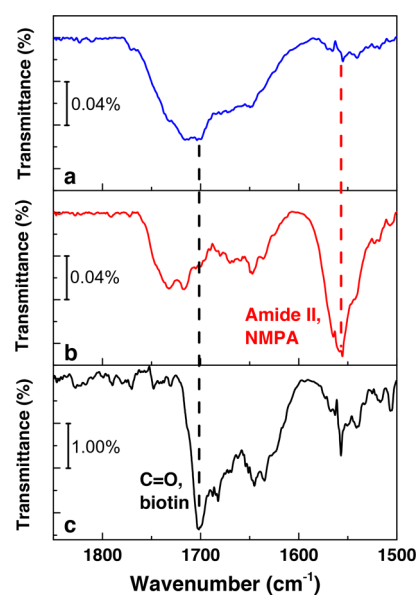

Figure 2. ATR-IR spectra in the region of 1850−1500 cm^{-1} for (a) 3MPA:11MUA biotinylated SAM, (b) NMPA:11MUA biotinylated SAM, and (c) pentylamine biotin. The black dashed line indicates the biotin ureido C═O stretching, whereas the red one highlights the NMPA amide II position.

SAMs as well as for the precursor used for biotinylation pentylamine-biotin (Figure 2c). A large absorption around 1700 cm^{-1} is observed in Figure 2a, consistent with the main band being associated to the ureido C═O stretching of the biotin ring (Figure 2c, indicated by a black dashed line). This is in agreement with the IR signals reported in the literature for biotin.[45] Such a large signal could be indicative of a higher amount of biotin immobilized on the 3MPA:11MUA SAM surface, which is compatible with the availability for

biotinylation of both 3MPA and 11MUA. In the case of the NMPA:11MUA SAM, no significant increased signal in this spectral area is recorded after biotinylation (Figure 2b). The comparison of the spectra of the two biotinylated SAMs clearly evidences that the two protocols generate completely different interphases, which is consistent with the representation given in Figure 1b,e: a higher amount of biotin is anchored on the 3MPA:11MUA sample, which leads to a less controlled chemical structure, particularly for the short-length chains. Here, unreacted chains (pristine 3MPA), biotin-conjugated 3MPA (B-3MPA), and only few molecules of NMPA generated during the last functionalization step with ethanol-amine can be assumed to be present on the basis of the acquired IR spectrum. Moreover, a large difference in the aliphatic N−H bending (amide II, highlighted with the red dashed line in Figure 2a,b) associated to NMPA can be observed between spectra in Figure 2a,b. In fact, the amide II absorption in Figure 2b is much more pronounced than in Figure 2a, being also quite sharp. This behavior has already been found in similar 3-mercapto-*N*-pentadecylpropionamide SAMs.[30] In fact, the inversion in the relative intensity between the amide I and amide II signals, as shown in Figure 2b, can be explained in terms of specific directions of the transition dipole moments for amide IR vibrations. NMPA chains in the biotinylated NMPA:11MUA SAMs are oriented in a nearly perpendicular configuration where the amide I dipole lies almost parallel to the gold surface thus being extremely attenuated for the IR surface selection rule and the amide II dipole is oriented perpendicularly thus resulting in a strong peak.[46−48] By contrast, the amide II absorption band in Figure 2a is not particularly intense because of limited formation of NMPA as well as possible different chain orientations.

Given the differences between the two biotinylated SAMs evidenced by ATR-IR study, SPR experiments were performed to explore their detection capability toward the SA target analyte. The typical sensograms (SPR angle shift vs time) obtained exposing the biotinylated SAM-modified gold chips to increasing concentrations of SA (500 pM−1.6 μM) are given in Figure 3. The alkanethiol packing on gold is $7.6 \cdot 10^{-10}$ mol/cm²;[49] hence, a number as high as $N = 10^{13}-10^{14}$ of
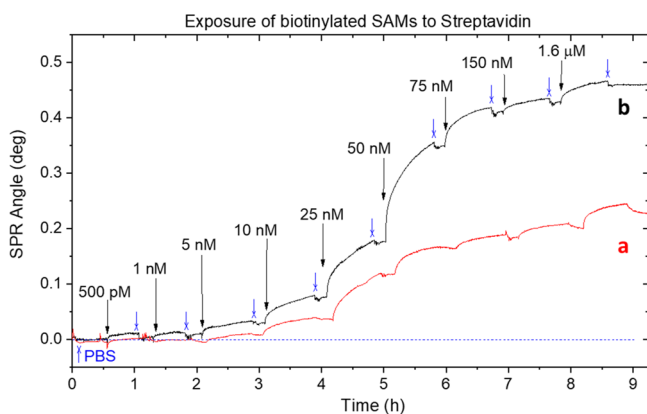

Figure 3. SPR real-time monitoring of streptavidin binding to biotinylated mixed SAMs obtained starting from the (a) 3MPA:11-MUA or (b) the NMPA:11MUA solutions. The black arrows indicate the injection of streptavidin solutions in the 500 pM−1.6 μM concentration range. The blue arrows indicate the PBS washing steps to remove the streptavidin excess. SPR angle values were measured taking as of zero level (offset) the angle measured in PBS.

biotins on the gold surface can be reasonably assumed. Considering that SA is a tetrameric protein capable of binding up to two biotins anchored on a surface, an $N/2$ maximum number of SA molecules is needed to saturate all the binding sites. The highest SA concentration chosen (1.6 μM) assured a supply of analyte molecules well in excess of the available binding sites.

The sensograms in Figure 3 show that a higher angle shift is generally observed at each SA exposure, even at low concentrations, for the NMPA:11MUA biotinylated SAM (Figure 3, curve b) as compared to the 3MPA:11MUA biotinylated SAM (Figure 3, curve a). This feature is better detailed with the analysis presented in Figure 4. Here, the SPR
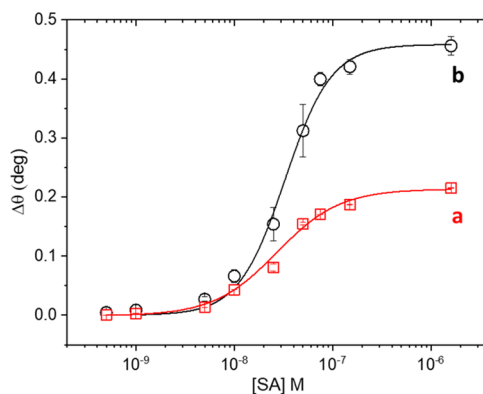

Figure 4. SPR angle shift response vs streptavidin concentration. Comparison of the responses of the two biotinylated SAMs: 3MPA:11MUA (a, red open squares) and NMPA:11MUA (b, black open circles). Reproducibility error bars are taken as one standard deviation over three replicates measured on three different SPR biofunctionalized slides. The solid lines are the result of the fitting (see main text for details).

angle shift response ($\Delta\theta$) versus the streptavidin concentration (semi-log scale) is shown for the two biotinylated SAMs. The reproducibility error bars are taken as one standard deviation over three replicates measured on three different SPR biofunctionalized slides. The solid lines in Figure 4 are the result of a fitting against the Hill's equation:[50,51]

$$Y = V_{max} \cdot \frac{X^n}{k^n + X^n} \qquad (1)$$

where $Y = \Delta\theta$, $X = [SA]$, n is the Hill parameter, and k is the apparent dissociation constant, i.e., the analyte concentration corresponding to half of the maximum response (V_{max}) or, equivalently, half-occupied binding sites. For the assay performed on the 3MPA:11MUA SAM (Figure 4, a) the following fitting parameters are derived: $k = (2.3 \pm 0.2) \times 10^{-8}$ M and $n = 1.5 \pm 0.1$. Considering that the dissociation constant k_d is equal to k^n, a value of 6.2×10^{-12} M was estimated. For the NMPA:11MUA SAM (Figure 4, b), the fitting parameters are $k = (3.3 \pm 0.2) \times 10^{-8}$ M and $n = 1.8 \pm 0.2$, resulting in a $k_d \approx 1.6 \times 10^{-14}$ M. The Hill parameter, n, reflects the degree of cooperativeness of the target molecules interacting with the binding sites; $n = 1$ holds for a non-cooperative binding, while $n > 1$ and $n < 1$ apply for positive and negative cooperativity, respectively.[52] For both systems a Hill coefficient $n > 1$ was observed, which means that a positive cooperativity in the biotin−streptavidin interaction occurred. This is in agreement with what was already reported.[51,53] From

the data in Figure 4, it can also be inferred that the biotinylated NMPA:11MUA SAM has a higher affinity toward SA, reaching k_d values similar to those reported for the biotin−SA binding in solution.[41,54]

The SPR study shows also a different SA coverage for the two SAMs. In fact, the SPR technique enables the evaluation of the surface coverage (Γ in ng/cm^2) by relating the plasmon resonance angle shift $\Delta\theta$ to the amount of adsorbed ligands by means of the de Feijter's equation (eq 2). Here, the surface coverage is estimated as the ratio of the optical thickness of the deposited ligand (D_0) and the refractive index increment (dn/dC).

$$\Gamma = D_0 \left(\frac{dn}{dC} \right)^{-1} \qquad (2)$$

where the optical thickness is equal to $D_0 = d(n - n_0) = dk\Delta\theta$ with d being the average layer thickness and k the wavelength-dependent sensitivity coefficient.[40,41] For thin layers and with a source wavelength of 670 nm, the product $k \times d \approx 1.0 \times 10^{-7}$ cm/deg. and $dn/dC \approx 0.182$ cm^3/g.[24] Therefore, eq 2 becomes:

$$\Gamma = \Delta\theta \times 550 \ (\text{ng/cm}^2) \qquad (2a)$$

A maximum surface coverage of $\Gamma = (114 \pm 4)$ ng/cm^2 was calculated from the V_{max} value obtained from the Hill's fitting of the dose curve (a) in Figure 4. It corresponds to $(1.14 \pm 0.04) \times 10^{12}$ molecules/cm^2. From the fitting of curve b in Figure 5, a maximum surface coverage of $\Gamma = 252 \pm 8$ ng/cm^2
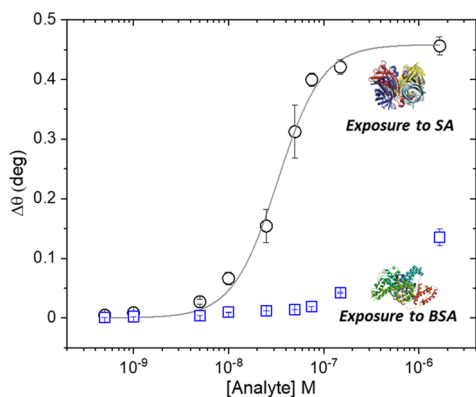

Figure 5. SPR angle shift vs analyte concentration for the biotinylated SAM (NMPA:11MUA) exposed to the affinity ligand, streptavidin (black open circles), and an interferent, BSA (blue open squares).

was calculated, corresponding to $(2.5 \pm 0.1) \times 10^{12}$ molecules/cm^2. The latter value is closer to a theoretical density of approximately 3.2×10^{12} molecules/cm^2 of highly packed streptavidin molecules of a size of $5.4 \times 5.8 \times 4.8$ nm.[37,55] Moreover, saturation is reached at approximately 100 nM, which corresponds to ca. 10^{12} SA in a 100 μL volume of the SPR cell. This shows that almost all the SA molecules in the available volume are attached to the surface. This is a rather important piece of evidence that shows how the diffusion of SA in the relatively large volume plays a very negligible role.

The biotinylated surfaces were tested also against a possible interferent, bovine serum albumin (BSA), to evaluate the selectivity of the system. In Figure 5, the SPR response $\Delta\theta$ to increasing BSA concentrations is reported for the biotinylated NMPA:11MUA SAM (blue squares) and it is compared with

the response to the target analyte (black circles). Nonspecific adsorption of BSA is observed only in the micromolar range though being below 28% of the SA response level at the same concentration. Moreover, the limit of detection (LOD) of the SA assay was estimated to be 2.6 ± 0.8 nM (see the Supporting Information for details). Over the same concentration range, the response observed for the 3MPA:11MUA biotinylated SAM (Figure 6, open circles) was considerably lower than that
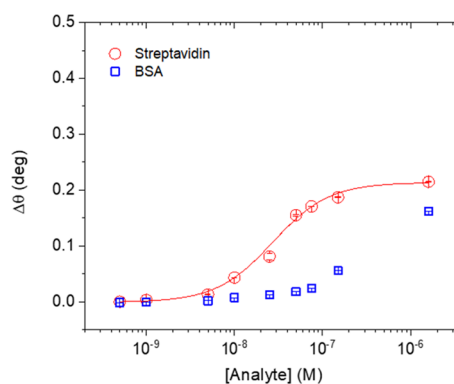

Figure 6. Angle shift vs analyte concentration for the 3MPA:11MUA biotinylated SAM. The SPR response is shown for both the affinity ligand and streptavidin (red circle) and for an interferent, BSA (blue squares).

reported when NMPA is used as alternative thiol. An LOD of 6 $\pm$ 1 nM was estimated in this case. Moreover, the exposure to BSA is particularly critical for the 3MPA:11MUA biotinylated SAM (Figure 6, open squares). In this case, at high concentrations, the responses to both the target analyte and the interferent are very similar indicating the significant contribution of nonspecific binding. An estimation on the surface coverage gained for BSA exposure was calculated to be 89 $\pm$ 1 ng/cm^2 and 74 $\pm$ 8 ng/cm^2 for biotinylated 3MPA:11MUA and NMPA:11MUA, respectively. Again, reduced absorption of BSA is demonstrated for the latter over the former. Comparable coverage (60−100 ng/cm^2) has been reported in similar assays in which BSA was used for nonspecific binding tests.[56,57] This is a good starting point for tests in real fluids considering that albumin represents a major component in sera.[58] Therefore, the different compositions of the two biotinylated surfaces seem to affect drastically the nonspecific binding as better selectivity is found for the SAM holding the hydroxyl terminal functionality on short chains (NMPA:11MUA-based sample), which could protect the surface from spurious physisorption.[19] The main figures of merit relevant to the two biotinylated surfaces for SA sensing are reported in Table 2 for direct comparison. It should also be highlighted that similar biotinylated SAMs employed in SPR sensors for SA detection achieve comparable[36] or even higher LODs in the order of 5−20 nM.[59,60] Lower detection limits could be reached by signal amplification with gold nano-particles.[61]

In order to provide a molecular explanation of the observed different performance levels, we performed MD simulations on a system reproducing a SAM resulting from a NMPA:11MUA functionalization strategy (SAM-1) and four systems mimicking a 3MPA:11MUA functionalization strategy (SAM-2, SAM-3, SAM-4, and SAM-5). Notice that the number of biotin-conjugated 3MPA (B-3MPA) increases in going from SAM-1 (number equal to 0) to SAM-5 (number equal to 654, Table

Table 2. Analytical Figures of Merit of the Two Different Biotinylated SAMs (3MPA:11MUA and NMPA:11MUA) for SA Detection[a]

sample	RSD%, n = 3	LOD (nM)	sensitivity (°/M)	selectivity ($\Delta\theta_{BSA}/\Delta\theta_{SA}$)
3MPA:11MUA SAM	±2	6 ± 1	$(4.9 \pm 0.2) \times 10^6$	0.75
NMPA:11MUA SAM	±1	2.6 ± 0.8	$(5.8 \pm 0.1) \times 10^6$	0.29

[a]The percentage relative standard deviation (RSD%) was estimated over $n = 3$ (n = number of independent experiments on three different biotinylated SPR chips). The limit of detection (LOD) and sensitivity (slope) were calculated from the linear fittings as reported in the Supporting Information (Figure S8). The selectivity was expressed as a ratio between the angle shift ($\Delta\theta$) observed for the interferent (BSA) over that for the analyte, taking both at the highest concentration (1.6 μM).

1). An in-depth analysis of the obtained trajectories was performed focusing the attention on biotinylated 11MUAs (hereinafter referred to as B-11MUAs), namely, the chains likely playing the major role in the biorecognition process.[62,63] More specifically, we computed for each system (i) the average number of stable H bonds (occupancy of >10%) that a B-11MUA establishes with the neighboring chains, (ii) the average value of root main square fluctuations (RMSF) computed for all the B-11MUAs belonging to the investigated system. The obtained data depict a trend illustrated in Figure 7: the higher the number of B-3MPAs in the system, the higher
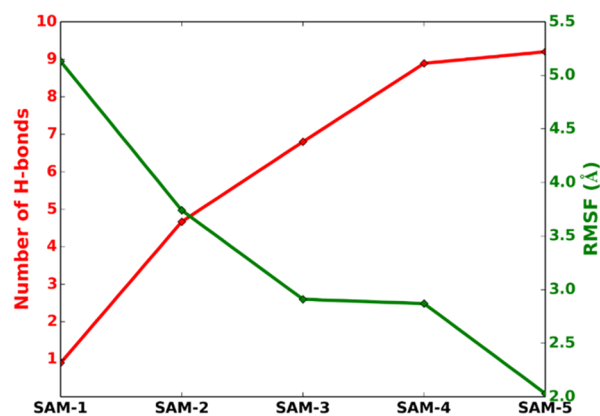

Figure 7. Dependence of the average number of stable H-bonds (occupancy of >10%) established by B-11MUA with neighboring chains (red line) and the average value of root main square fluctuations (RMSF) per B-11MUA (green line) on the five simulated systems.

the average number of H bonds established by B-11MUA. More specifically, an in-depth visual inspection of the trajectories revealed that long (B-11MUA) and short (B-3MPA) biotinylated chains can strongly interact via H bonds involving their biotin portion. In other words, increasing the number of B-3MPAs in the system increases the risk that B-11MUAs is involved in strong H-bond interactions before SA anchoring takes place. As evident in comparing the computed RMSF values for all the investigated systems (Figure 7), such interchain interactions are responsible for significant reduction of the B-11MUA conformational freedom and hence availability to bind SA. Building on these data, it is possible to speculate that, by avoiding the interactions between B-11MUA and B-3MPA, the NMPA:11MUA functionalization strategy allows for the development of a mixed SAM whose B-11MUAs are much more accessible for the SA binding.

CONCLUSIONS

We have designed and prepared a highly ordered and selective biotinylated mixed SAM starting with the ex situ synthesis of a short-chain dilution thiol. In this way, biotin immobilization was specifically driven only on the long-chain alkyl thiol. The protocol efficiency was demonstrated by both ATR-IR and SPR characterizations by comparison with a very similar biotinylated SAM prepared from commercial sources. Using the SA/biotin pair as a model system, the importance of proper tuning of surface moieties was proven on the sensing figures of merit. Finally, MD computations suggest a link between the observed performance and the occurrence of interchain interactions within the investigated mixed SAMs. It was demonstrated that ex situ synthesis of NMPA limits considerably the occurrence of nonspecific binding, thus improving the biosensing platform selectivity. This strategy, based on the harmonic use of experimental and theoretical approaches, could pave the way for the design and development of more robust and reliable interfaces for the further assembly of more sophisticated biorecognition elements of application in ultrasensitive devices. Further studies based on scanning probe microscopies combined with surface spectroscopic techniques will be performed to shed light on the modified surface architectures and biomolecule immobilization.

ASSOCIATED CONTENT

Ⓢ Supporting Information

The Supporting Information is available free of charge at https://pubs.acs.org/doi/10.1021/acsomega.0c01717.

> Schemes of SAMs, synthesis of NMPA, SPR and ATR-IR protocols, IR assignments, and MD simulations (PDF)

AUTHOR INFORMATION

Corresponding Authors

Francesco Leonetti − Dipartimento di Farmacia − Scienze del Farmaco, Università degli Studi di Bari Aldo Moro, 70125 Bari, Italy; Email: francesco.leonetti@uniba.it

Giuseppe Felice Mangiatordi − CNR − Institute of Crystallography, 70126 Bari, Italy; ⓞ orcid.org/0000-0003-4042-2841; Email: giuseppe.mangiatordi@ic.cnr.it

Rosaria Anna Picca − CSGI, Unità di Bari, 70125 Bari, Italy; Dipartimento di Chimica, Università degli Studi di Bari Aldo Moro, 70125 Bari, Italy; ⓞ orcid.org/0000-0001-8033-098X; Email: rosaria.picca@uniba.it

Authors

Davide Blasi − CSGI, Unità di Bari, 70125 Bari, Italy

Lucia Sarcina − Dipartimento di Chimica, Università degli Studi di Bari Aldo Moro, 70125 Bari, Italy

Angelo Tricase − Dipartimento di Chimica, Università degli Studi di Bari Aldo Moro, 70125 Bari, Italy

Angela Stefanachi − *Dipartimento di Farmacia − Scienze del Farmaco, Università degli Studi di Bari Aldo Moro, 70125 Bari, Italy;* orcid.org/0000-0002-9430-7972

Domenico Alberga − *CINECA, 40033 Casalecchio di Reno, Italy*

Kyriaki Manoli − *CSGI, Unità di Bari, 70125 Bari, Italy; Dipartimento di Chimica, Università degli Studi di Bari Aldo Moro, 70125 Bari, Italy;* orcid.org/0000-0002-7600-0977

Gaetano Scamarcio − *Dipartimento di Fisica "M. Merlin", Università degli Studi di Bari Aldo Moro, 70126 Bari, Italy; IFN CNR, Sede secondaria di Bari, 70126 Bari, Italy*

Luisa Torsi − *CSGI, Unità di Bari, 70125 Bari, Italy; Dipartimento di Chimica, Università degli Studi di Bari Aldo Moro, 70125 Bari, Italy; Physics and Center for Functional Materials, Faculty of Science and Engineering, Åbo Akademi University, 20500 Åbo, Finland*

Complete contact information is available at:
https://pubs.acs.org/10.1021/acsomega.0c01717

Author Contributions

◆D.B., L.S., and A.T. contributed equally as first authors to the work. D.B. designed the experiments and contributed to data interpretation. L.S. performed SPR experiments and analyzed the data under the supervision of K.M. A.T. performed ATR-IR characterization and analyzed the spectra under the supervision of G.S. A.S. carried out the synthesis of NMPA under the supervision of F.L. D.A. performed MD simulations under the supervision of G.F.M. R.A.P. conceived the study, contributed to data analysis, and wrote the first draft of the manuscript. L.T. supervised all the activities, coordinated the work, and reviewed the manuscript that was approved by all the authors.

Notes

The authors declare no competing financial interest.

REFERENCES

(1) Wang, B.; Akiba, U.; Anzai, J. I. Recent Progress in Nanomaterial-Based Electrochemical Biosensors for Cancer Biomarkers: A Review. *Molecules* **2017**, *22*, 1048.

(2) Samanta, D.; Sarkar, A. Immobilization of Bio-Macromolecules on Self-Assembled Monolayers: Methods and Sensor Applications. *Chem. Soc. Rev.* **2011**, *40*, 2567−2592.

(3) Schwartz, D. K. Mechanisms and Kinetics of Self-Assembled Monolayer Formation. *Annu. Rev. Phys. Chem.* **2001**, *52*, 107−137.

(4) Nicosia, C.; Huskens, J. Reactive Self-Assembled Monolayers: From Surface Functionalization to Gradient Formation. *Mater. Horiz.* **2014**, *1*, 32−45.

(5) Nuzzo, R. G.; Allara, D. L. Adsorption of Bifunctional Organic Disulfides on Gold Surfaces. *J. Am. Chem. Soc.* **1983**, *105*, 4481−4483.

(6) Love, J. C.; Estroff, L. A.; Kriebel, J. K.; Nuzzo, R. G.; Whitesides, G. M. Self-Assembled Monolayers of Thiolates on Metals as a Form of Nanotechnology. *Chem. Rev.* **2005**, *105*, 1103−1170.

(7) Kawaguchi, T.; Shankaran, D. R.; Kim, S. J.; Gobi, K. V.; Matsumoto, K.; Toko, K.; Miura, N. Fabrication of a Novel Immunosensor Using Functionalized Self-Assembled Monolayer for Trace Level Detection of TNT by Surface Plasmon Resonance. *Talanta* **2007**, *72*, 554−560.

(8) Macchia, E.; Manoli, K.; Holzer, B.; Di Franco, C.; Ghittorelli, M.; Torricelli, F.; Alberga, D.; Mangiatordi, G. F.; Palazzo, G.; Scamarcio, G.; Torsi, L. Single-Molecule Detection with a Millimetre-Sized Transistor. *Nat. Commun.* **2018**, *9*, 3223.

(9) Macchia, E.; Tiwari, A.; Manoli, K.; Holzer, B.; Ditaranto, N.; Picca, R. A.; Cioffi, N.; Di Franco, C.; Scamarcio, G.; Palazzo, G.; Torsi, L. Label-Free and Selective Single-Molecule Bioelectronic Sensing with a Millimeter-Wide Self-Assembled Monolayer of Anti-Immunoglobulins. *Chem. Mater.* **2019**, *31*, 6476−6483.

(10) Macchia, E.; Manoli, K.; Holzer, B.; Di Franco, C.; Picca, R. A.; Cioffi, N.; Scamarcio, G.; Palazzo, G.; Torsi, L. Selective Single-Molecule Analytical Detection of C-Reactive Protein in Saliva with an Organic Transistor. *Anal. Bioanal. Chem.* **2019**, *411*, 4899−4908.

(11) Macchia, E.; Sarcina, L.; Picca, R. A.; Manoli, K.; Di Franco, C.; Scamarcio, G.; Torsi, L. Ultra-Low HIV-1 P24 Detection Limits with a Bioelectronic Sensor. *Anal. Bioanal. Chem.* **2020**, *412*, 811−818.

(12) Abbas, A.; Linman, M. J.; Cheng, Q. New Trends in Instrumental Design for Surface Plasmon Resonance-Based Biosensors. *Biosens. Bioelectron.* **2011**, *26*, 1815−1824.

(13) Spinke, J.; Liley, M.; Schmitt, F. J.; Guder, H.-J.; Angermaier, L.; Knoll, W. Molecular Recognition at Self-Assembled Monolayers: Optimization of Surface Functionalization. *J. Chem. Phys.* **1993**, *99*, 7012−7019.

(14) Frederix, F.; Bonroy, K.; Laureyn, W.; Reekmans, G.; Campitelli, A.; Dehaen, W.; Maes, G. Enhanced Performance of an Affinity Biosensor Interface Based on Mixed Self-Assembled Monolayers of Thiols on Gold. *Langmuir* **2003**, *19*, 4351−4357.

(15) Lee, J. W.; Sim, S. J.; Cho, S. M.; Lee, J. Characterization of a Self-Assembled Monolayer of Thiol on a Gold Surface and the Fabrication of a Biosensor Chip Based on Surface Plasmon Resonance for Detecting Anti-GAD Antibody. *Biosens. Bioelectron.* **2005**, *20*, 1422−1427.

(16) Garifullina, A.; Shen, A. Q. Optimized Immobilization of Biomolecules on Nonspherical Gold Nanostructures for Efficient Localized Surface Plasmon Resonance Biosensing. *Anal. Chem.* **2019**, *91*, 15090−15098.

(17) Tsai, W.-C.; Li, I.-C. SPR-Based Immunosensor for Determining Staphylococcal Enterotoxin A. *Sens. Actuators, B* **2009**, *136*, 8−12.

(18) Mauriz, E.; García-Fernández, M. C.; Lechuga, L. M. Towards the Design of Universal Immunosurfaces for SPR-Based Assays: A Review. *TrAC, Trends Anal. Chem.* **2016**, *79*, 191−198.

(19) Briand, E.; Salmain, M.; Herry, J.-M.; Perrot, H.; Compère, C.; Pradier, C.-M. Building of an Immunosensor: How Can the Composition and Structure of the Thiol Attachment Layer Affect the Immunosensor Efficiency? *Biosens. Bioelectron.* **2006**, *22*, 440−448.

(20) Ataman Sadık, D.; Eksi-Kocak, H.; Ertaş, G.; Boyacı, İ. H.; Mutlu, M. Mixed-Monolayer of N-Hydroxysuccinimide-Terminated Cross-Linker and Short Alkanethiol to Improve the Efficiency of Biomolecule Binding for Biosensing. *Surf. Interface Anal.* **2018**, *50*, 866−878.

(21) Bhadra, P.; Shajahan, M. S.; Bhattacharya, E.; Chadha, A. Studies on Varying N-Alkanethiol Chain Lengths on a Gold Coated

Surface and Their Effect on Antibody-Antigen Binding Efficiency. *RSC Adv.* **2015**, *5*, 80480−80487.

(22) Rodriguez-Emmenegger, C.; Avramenko, O. A.; Brynda, E.; Skvor, J.; Alles, A. B. Poly(HEMA) Brushes Emerging as a New Platform for Direct Detection of Food Pathogen in Milk Samples. *Biosens. Bioelectron.* **2011**, *26*, 4545−4551.

(23) Leo, N.; Liu, J.; Archbold, I.; Tang, Y.; Zeng, X. Ionic Strength, Surface Charge, and Packing Density Effects on the Properties of Peptide Self-Assembled Monolayers. *Langmuir* **2017**, *33*, 2050−2058.

(24) Holzer, B.; Manoli, K.; Ditaranto, N.; Macchia, E.; Tiwari, A.; Di Franco, C.; Scamarcio, G.; Palazzo, G.; Torsi, L. Characterization of Covalently Bound Anti-Human Immunoglobulins on Self-Assembled Monolayer Modified Gold Electrodes. *Adv. Biosyst.* **2017**, *1*, 1700055.

(25) Picca, R. A.; Manoli, K.; Macchia, E.; Sarcina, L.; Di Franco, C.; Cioffi, N.; Blasi, D.; Österbacka, R.; Torricelli, F.; Scamarcio, G.; Torsi, L. Ultimately Sensitive Organic Bioelectronic Transistor Sensors by Materials and Device Structures' Design. *Adv. Funct. Mater.* **2019**, 1904513.

(26) Picca, R. A.; Blasi, D.; Macchia, E.; Manoli, K.; Di Franco, C.; Scamarcio, G.; Torricelli, F.; Zurutuza, A.; Napal, I.; Centeno, A.; Torsi, L. A Label-Free Immunosensor Based on a Graphene Water-Gated Field-Effect Transistor. In *2019 IEEE 8th International Workshop on Advances in Sensors and Interfaces (IWASI)*; IEEE, 2019; pp 136−138.

(27) Patel, N.; Davies, M. C.; Hartshorne, M.; Heaton, R. J.; Roberts, C. J.; Tendler, S. J. B.; Williams, P. M. Immobilization of Protein Molecules onto Homogeneous and Mixed Carboxylate-Terminated Self-Assembled Monolayers. *Langmuir* **1997**, *13*, 6485−6490.

(28) Arya, S. K.; Lee, K. C.; Dah'Alan, D. B.; Daniel; Rahman, A. R. A. Breast Tumor Cell Detection at Single Cell Resolution Using an Electrochemical Impedance Technique. *Lab Chip* **2012**, *12*, 2362−2368.

(29) Carot, M. L.; Macagno, V. A.; Paredes-Olivera, P.; Patrito, E. M. Structure of Mixed Carboxylic Acid Terminated Self-Assembled Monolayers: Experimental and Theoretical Investigation. *J. Phys. Chem. C* **2007**, *111*, 4294−4304.

(30) Clegg, R. S.; Hutchison, J. E. Hydrogen-Bonding, Self-Assembled Monolayers: Ordered Molecular Films for Study of Through-Peptide Electron Transfer. *Langmuir* **1996**, *12*, 5239−5243.

(31) Lewis, P. A.; Smith, R. K.; Kelly, K. F.; Bumm, L. A.; Reed, S. M.; Clegg, R. S.; Gunderson, J. D.; Hutchison, J. E.; Weiss, P. S. The Role of Buried Hydrogen Bonds in Self-Assembled Mixed Composition Thiols on Au{111}. *J. Phys. Chem. B* **2001**, *105*, 10630−10636.

(32) Kim, M.; Hohman, J. N.; Serino, A. C.; Weiss, P. S. Structural Manipulation of Hydrogen-Bonding Networks in Amide-Containing Alkanethiolate Monolayers via Electrochemical Processing. *J. Phys. Chem. C* **2010**, *114*, 19744−19751.

(33) Thomas, J. C.; Goronzy, D. P.; Dragomiretskiy, K.; Zosso, D.; Gilles, J.; Osher, S. J.; Bertozzi, A. L.; Weiss, P. S. Mapping Buried Hydrogen-Bonding Networks. *ACS Nano* **2016**, *10*, 5446−5451.

(34) Meillan, M.; Buffeteau, T.; Le Bourdon, G.; Thomas, L.; Degueil, M.; Heuzé, K.; Bennetau, B.; Vellutini, L. Mixed Self-Assembled Monolayers with Internal Urea Group on Silica Surface. *ChemistrySelect* **2017**, *2*, 11868−11874.

(35) Cheung, K. M.; Stemer, D. M.; Zhao, C.; Young, T. D.; Belling, J. N.; Andrews, A. M.; Weiss, P. S. Chemical Lift-Off Lithography of Metal and Semiconductor Surfaces. *ACS Mater. Lett.* **2020**, *2*, 76−83.

(36) Hong, M.-Y.; Lee, D.; Kim, H.-S. Kinetic and Equilibrium Binding Analysis of Protein-Ligand Interactions at Poly(Amidoamine) Dendrimer Monolayers. *Anal. Chem.* **2005**, *77*, 7326−7334.

(37) Morgan, H.; Taylor, D. M.; D'Silva, C. Surface Plasmon Resonance Studies of Chemisorbed Biotin-Streptavidin Multilayers. *Thin Solid Films* **1992**, *209*, 122−126.

(38) Spinke, J.; Liley, M.; Guder, H. J.; Angermaier, L.; Knoll, W. Molecular Recognition at Self-Assembled Monolayers: The Con-

struction of Multicomponent Multilayers. *Langmuir* **1993**, *9*, 1821−1825.

(39) Nelson, K. E.; Gamble, L.; Jung, L. S.; Boeckl, M. S.; Naeemi, E.; Golledge, S. L.; Sasaki, T.; Castner, D. G.; Campbell, C. T.; Stayton, P. S. Surface Characterization of Mixed Self-Assembled Monolayers Designed for Streptavidin Immobilization. *Langmuir* **2001**, *17*, 2807−2816.

(40) BioNavis. *MP-SPR Navi LayerSolver User Manual. MP-SPR user Man.* 2015.

(41) Dubacheva, G. V.; Araya-Callis, C.; Geert Volbeda, A.; Fairhead, M.; Codée, J.; Howarth, M.; Richter, R. P. Controlling Multivalent Binding through Surface Chemistry: Model Study on Streptavidin. *J. Am. Chem. Soc.* **2017**, *139*, 4157−4167.

(42) Phillips, J. C.; Braun, R.; Wang, W.; Gumbart, J.; Tajkhorshid, E.; Villa, E.; Chipot, C.; Skeel, R. D.; Kalé, L.; Schulten, K. Scalable Molecular Dynamics with NAMD. *J. Comput. Chem.* **2005**, *26*, 1781−1802.

(43) Frey, B. L.; Corn, R. M. Covalent Attachment and Derivatization of Poly(L-Lysine) Monolayers on Gold Surfaces As Characterized by Polarization-Modulation FT-IR Spectroscopy. *Anal. Chem.* **1996**, *68*, 3187−3193.

(44) Moldovan, C.; Mihailescu, C.; Stan, D.; Ruta, L.; Iosub, R.; Gavrila, R.; Purica, M.; Vasilica, S. Characterization of Self-Assembled Monolayers (SAMs) on Silicon Substrate Comparative with Polymer Substrate for Escherichia Coli O157:H7 Detection. *Appl. Surf. Sci.* **2009**, *255*, 8953−8959.

(45) Lapin, N. A.; Chabal, Y. J. Infrared Characterization of Biotinylated Silicon Oxide Surfaces, Surface Stability, and Specific Attachment of Streptavidin. *J. Phys. Chem. B* **2009**, *113*, 8776−8783.

(46) Clegg, R. S.; Reed, S. M.; Smith, R. K.; Barron, B. L.; Rear, J. A.; Hutchison, J. E. The Interplay of Lateral and Tiered Interactions in Stratified Self-Organized Molecular Assemblies. *Langmuir* **1999**, *15*, 8876−8883.

(47) Bieri, M.; Bürgi, T. Adsorption Kinetics, Orientation, and Self-Assembling of N-Acetyl-l-Cysteine on Gold: A Combined ATR-IR, PM-IRRAS, and QCM Study. *J. Phys. Chem. B* **2005**, *109*, 22476−22485.

(48) Greenler, R. G. Infrared Study of Adsorbed Molecules on Metal Surfaces by Reflection Techniques. *J. Chem. Phys.* **1966**, *44*, 310−315.

(49) Widrig, C. A.; Chung, C.; Porter, M. D. The Electrochemical Desorption of N-Alkanethiol Monolayers from Polycrystalline Au and Ag Electrodes. *J. Electroanal. Chem.* **1991**, *310*, 335−359.

(50) Barlow, R.; Blake, J. F. Hill Coefficients and the Logistic Equation. *Trends Pharmacol. Sci.* **1989**, *10*, 440−441.

(51) Martinez, K. L.; Meyer, B. H.; Hovius, R.; Lundstrom, K.; Vogel, H. Ligand Binding to G Protein-Coupled Receptors in Tethered Cell Membranes. *Langmuir* **2003**, *19*, 10925−10929.

(52) Weiss, J. N. The Hill Equation Revisited: Uses and Misuses. *FASEB J.* **1997**, *11*, 835−841.

(53) Mulla, M. Y.; Tuccori, E.; Magliulo, M.; Lattanzi, G.; Palazzo, G.; Persaud, K.; Torsi, L. Capacitance-Modulated Transistor Detects Odorant Binding Protein Chiral Interactions. *Nat. Commun.* **2015**, *6*, 6010.

(54) Kraehenbuhl, J.-P.; Bonnard, C. [75] Purification and characterization of membrane proteins. *Methods Enzymol.* **1990**, *184*, 629−641.

(55) Mullett, W. M.; Lai, E. P. C.; Yeung, J. M. Surface Plasmon Resonance-Based Immunoassays. *Methods* **2000**, *22*, 77−91.

(56) Liang, H.; Miranto, H.; Granqvist, N.; Sadowski, J. W.; Viitala, T.; Wang, B.; Yliperttula, M. Surface Plasmon Resonance Instrument as a Refractometer for Liquids and Ultrathin Films. *Sens. Actuators, B* **2010**, *149*, 212−220.

(57) Silin, V.; Weetall, H.; Vanderah, D. J. SPR Studies of the Nonspecific Adsorption Kinetics of Human IgG and BSA on Gold Surfaces Modified by Self-Assembled Monolayers (SAMs). *J. Colloid Interface Sci.* **1997**, *185*, 94−103.

(58) Majorek, K. A.; Porebski, P. J.; Dayal, A.; Zimmerman, M. D.; Jablonska, K.; Stewart, A. J.; Chruszcz, M.; Minor, W. Structural and

Immunologic Characterization of Bovine, Horse, and Rabbit Serum Albumins. *Mol. Immunol.* **2012**, *52*, 174−182.

(59) Seto, H.; Yamashita, C.; Kamba, S.; Kondo, T.; Hasegawa, M.; Matsuno, M.; Ogawa, Y.; Hoshino, Y.; Miura, Y. Biotinylation of Silicon and Nickel Surfaces and Detection of Streptavidin as Biosensor. *Langmuir* **2013**, *29*, 9457−9463.

(60) Focsan, M.; Campu, A.; Craciun, A.-M.; Potara, M.; Leordean, C.; Maniu, D.; Astilean, S. A Simple and Efficient Design to Improve the Detection of Biotin-Streptavidin Interaction with Plasmonic Nanobiosensors. *Biosens. Bioelectron.* **2016**, *86*, 728−735.

(61) Guo, X. Surface Plasmon Resonance Based Biosensor Technique: A Review. *J. Biophotonics* **2012**, *5*, 483−501.

(62) White, R. J.; Phares, N.; Lubin, A. A.; Xiao, Y.; Plaxco, K. W. Optimization of Electrochemical Aptamer-Based Sensors via Optimization of Probe Packing Density and Surface Chemistry. *Langmuir* **2008**, *24*, 10513−10518.

(63) Bedford, E. E.; Boujday, S.; Humblot, V.; Gu, F. X.; Pradier, C.-M. Effect of SAM Chain Length and Binding Functions on Protein Adsorption: β-Lactoglobulin and Apo-Transferrin on Gold. *Colloids Surf., B* **2014**, *116*, 489−496.